Supporting Information

Stretchable Sodium-Ion Capacitors Based on Coaxial CNT Supported $Na_2Ti_3O_7$ with High Capacitance Contribution

Jin Chen, Hongchun Mu, Jianlong Ding, Yifan Zhang, Wenqiang Wang and Gengchao Wang**

Experimental section

Preparation of ACM/CB-Ag NWs stretchable current collector

Typically, 1 g CB (BP 2000, Cabot) was evenly dispersed in 20 ml *N,N*-Dimethylformamide (DMF, ⩾99.5%, Aldrich) after grinding and ball milling. 1 g ACM (AR51, Nippon Zeon) was dissolved in 10 ml DMF. CB dispersion, silver nanowires ink (Ag NWs, Zhejiang Kechuang Advanced Material Co., Ltd) and crosslinking agent Triethylenetetramine (TETA) were added to ACM solution in turn and continuously stirred for 4 h, and control the weight of the CB, Ag NWs and TETA to 10 wt%, 3 wt% and 8 wt% of ACM respectively. The same cross-linking step of BCNF-*p*ACM QPE was repeated in next operation. Then, the stretchable current collector was taken out of the PTFE plate for later use. Reference ACM/CB and ACM/Ag NWs were prepared similarly without the addition of Ag NWs and CB, respectively.

Half cells and three-electrode systems:

For the negative/positive electrodes, 80 wt% of *n*CNT@NTO or AC, 10 wt% of carbon black, and 10 wt% of polyacrylic acid (PAA, MW = 450000) were homogeneously mixed in NMP through grinding for 1 h. Then the abovementioned slurry was coated onto a polished copper/aluminum foil or 1 x 2 cm ACM/CB-Ag NWs stretchable current collector and dried in a vacuum oven at 80 °C for 12 h. Finally, the specific capacity was calculated based on the mass of active materials and 2.75 mg cm^{-2} of AC and 1.1 mg cm^{-2} of *n*CNT@NTO were obtained. CR2032-type half cells

assembly and the whole electrochemical test was assembled in a glove box filled with argon atmosphere. Among them, AC was tested by a three-electrode system within a voltage window of 2.5 - 4.2 V, in which platinum net as counter electrode and sodium sheet as reference electrode.

Electrochemical Measurements:

SSIC devices was tested in a potential window of 1-4 V. The specific power densities (P, W kg^{-1} or W cm^{-3}) and specific energy densities (E, Wh kg^{-1} or Wh cm^{-3}) of the SSIC were calculated via the following formula:

$$\Delta V = \frac{V_{max} + V_{min}}{2} \tag{3}$$

$$C_m = \frac{I_m}{\Delta V} \times \Delta t \tag{4}$$

$$E = \int_{t1}^{t2} IVdt == \Delta V \times I_m \times t \tag{5}$$

$$P = \frac{E}{t} = \Delta V \times I_m \tag{6}$$

where V_{min} and V_{max} are the potential at the initial and final charge curves during galvanostatic measurements, respectively; I_m represent the current density normalized by the total electro-active mass in both electrodes (A g^{-1}) or the geometric area of flexible electrode (A cm^{-2}); C_m is the specific capacitance of the device.

Materials characterization

Sample morphologies were characterized via the field-emission scanning electron microscopy (FE-SEM, Hitachi S4800) and transmission electron microscopy (TEM, JEOL JEM-2100). Powder XRD was conducted on a Rigaku D/Max 2550 VB/PC X diffractometer with Cu Kα radiation. Fourier transform infrared spectroscopy (FTIR) was performed on a Nicolet 6700. Raman spectroscopy was carried out using a Laser Micro-Raman Spectrometer (Invia Reflex). The thermal gravimetric analysis (TG) was performed on a Thermogravimetric Analyzer-Gas Chromatograph-Mass Spectrometer (NETZSCH, TG209F1-GC) with a heating rate of 10 °C min^{-1} under air atmosphere. The tensile tests and cyclic tensile test were carried out at a strain rate of 30- and 10-mm min^{-1} via a high precision dynamometer (M7, Mark-10). The resistance of

stretchable current collector was measured by a precision DC low resistance tester (REK, RK2514).

Electrolyte uptake:

The electrolyte uptake was calculated using the following equation:

$$Electrolyte\ uptake = \frac{(w_w - w_d)}{w_d} \times 100\% \quad (1)$$

Where w_d and w_w are the weight of the film after drying in 60 ℃ vacuum oven and the weight of the film immersed in electrolyte.

Ionic conductivity:

The ionic conductivity was measured by electrochemical impedance spectroscopy (EIS) method and calculated using the following equation:

$$\sigma = \frac{L}{R \times S} \quad (2)$$

where L and S are the thickness and area of the BCNF-*p*ACM, respectively, and R is the bulk ohmic resistance of the BCNF-*p*ACM. The test conditions are under open circuit voltage, frequency range is 0.1 Hz-1 MHz, and amplitude is 10 mV.

Results and discussion

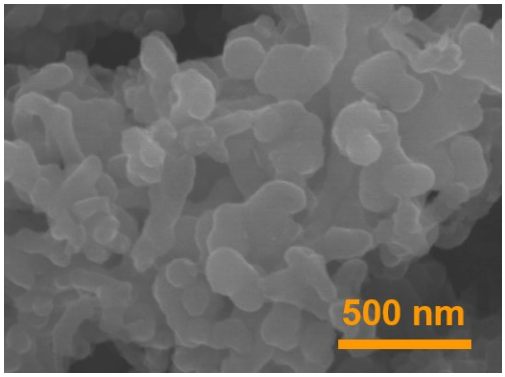

Fig. S1 FESEM image of NTO

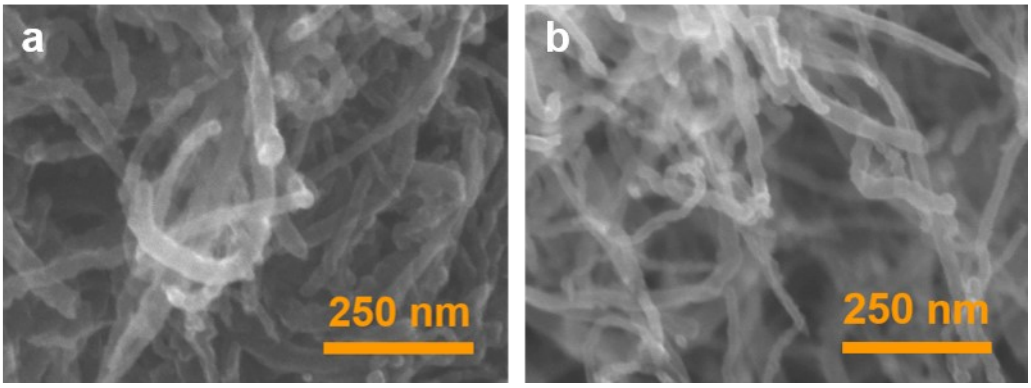

Fig. S2 FESEM images of (a) *a*CNT and (b) *n*CNT.

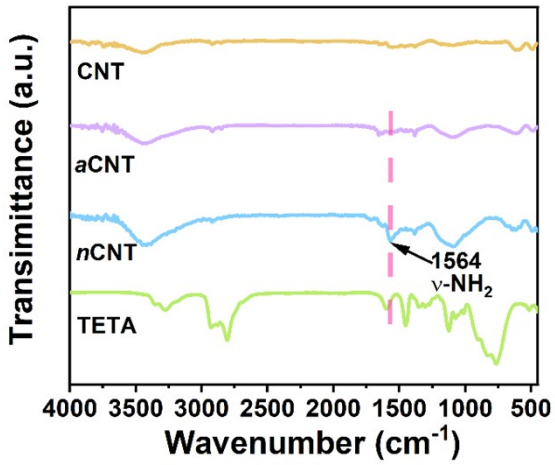

Fig. S3 FTIR spectra of pristine CNT, *a*CNT, *n*CNT and TETA.

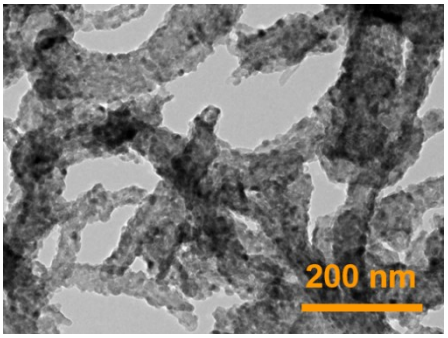

Fig. S4 TEM image of CNT@NTO.

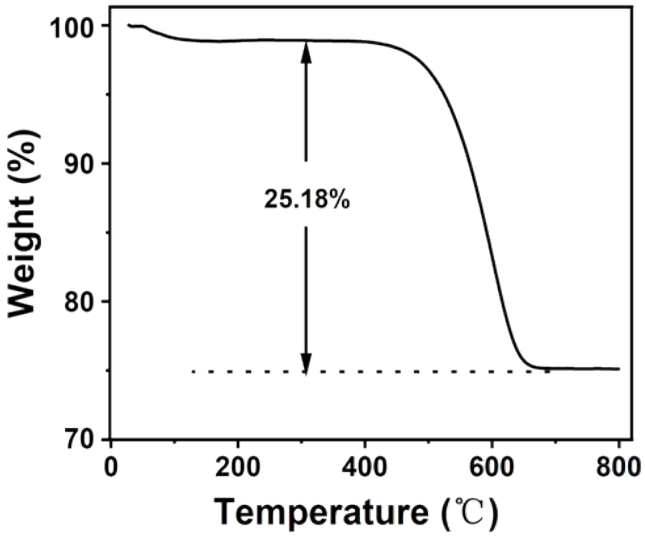

Fig. S5 TGA curve of *n*CNT@NTO in air atmosphere.

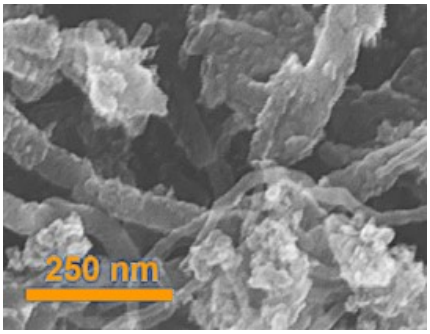

Fig. S6 FESEM image of *a*CNT/NTO without TETA.

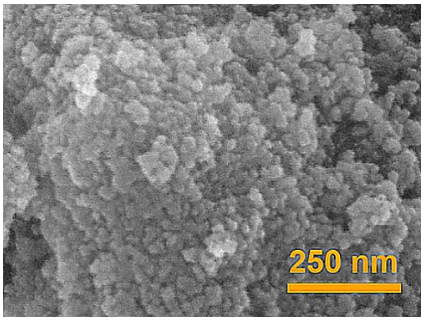

Fig. S7 FESEM image of *n*NTO with TETA.

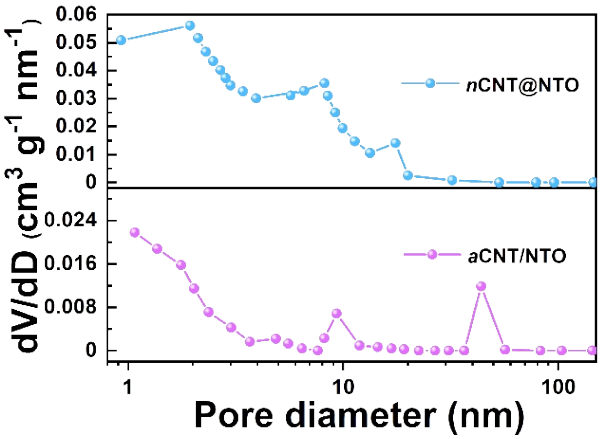

Fig. S8 Pore size distribution of *a*CNT/NTO and *n*CNT@NTO.

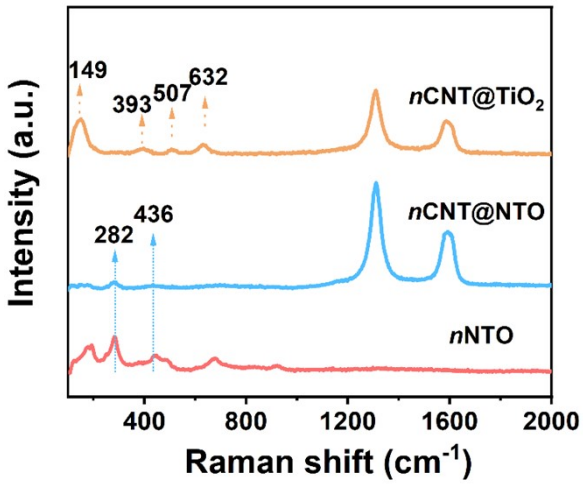

Fig. S9 Raman spectra of *n*NTO, *n*CNT@TiO_2, and *n*CNT@NTO.

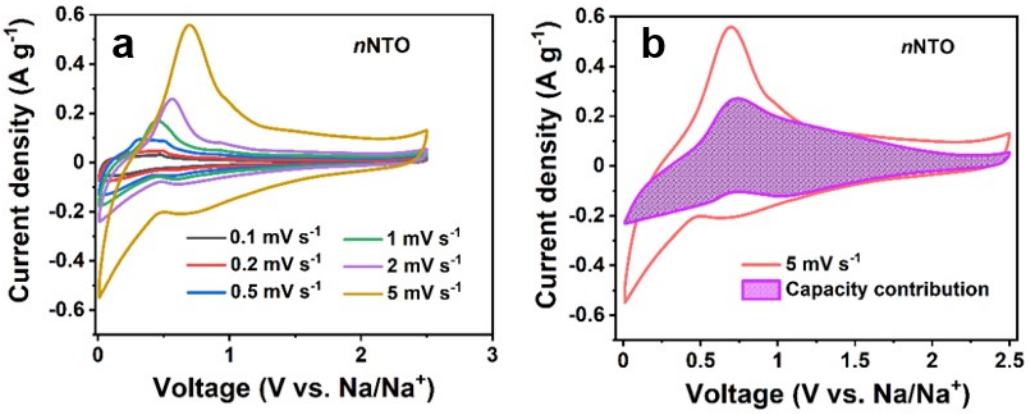

Fig. S10 (a) CV curves of *n*NTO at different scan rates. (b) CV curve of *n*NTO at a scan rate of 5 mV s^{-1}, corresponding capacitive contribution (shadow region).

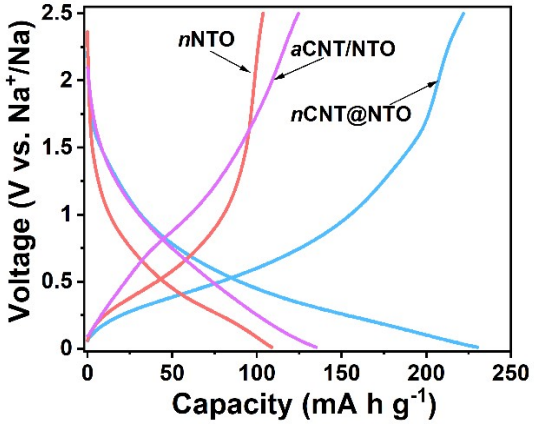

Fig. S11 Galvanostatic discharge/charge profiles at a rate of 0.2 A g^{-1} of *n*NTO, *a*CNT/NTO, and *n*CNT@NTO.

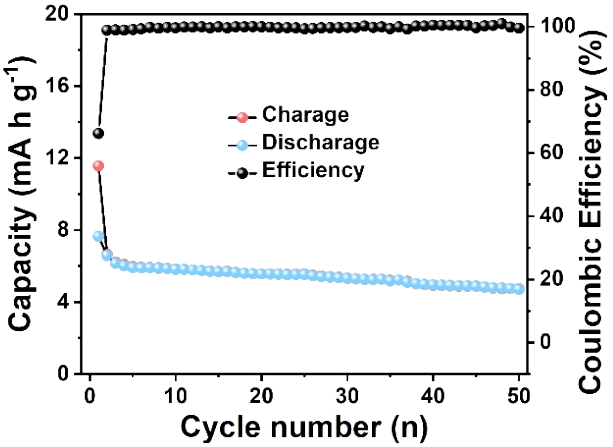

Fig. S12 Cycling performance of *n*CNT at 0.2 A g^{-1}.

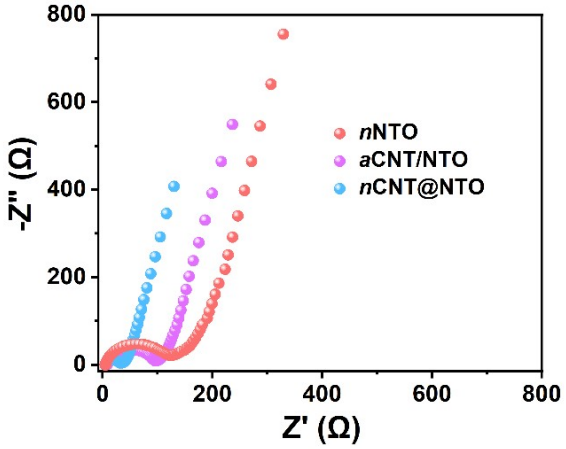

Fig. S13 The Nyquist plots of *n*NTO, *a*CNT/NTO, and *n*CNT@NTO.

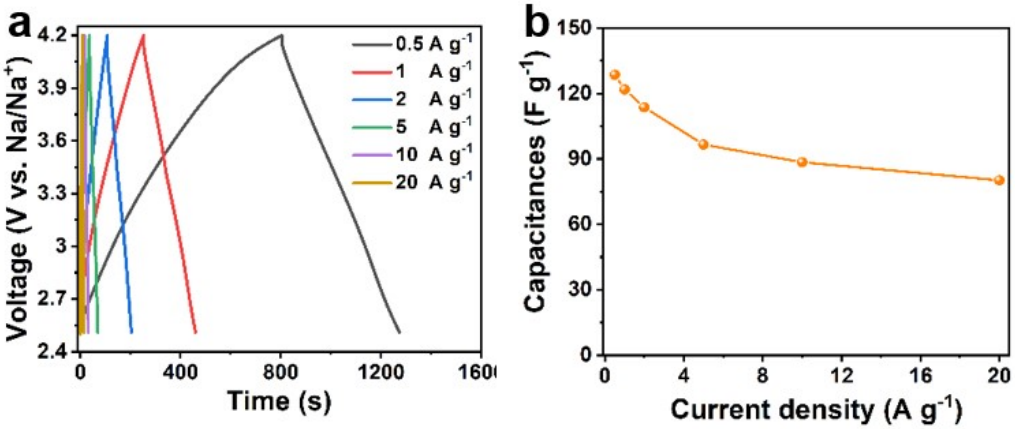

Fig. S14 Electrochemical performance of AC electrode in three-electrode system within a voltage window of 2.5 - 4.2 V. (a) Galvanostatic charge-discharge curves at various densities, (b) Corresponding specific capacitance calculated from discharge curves at various densities.

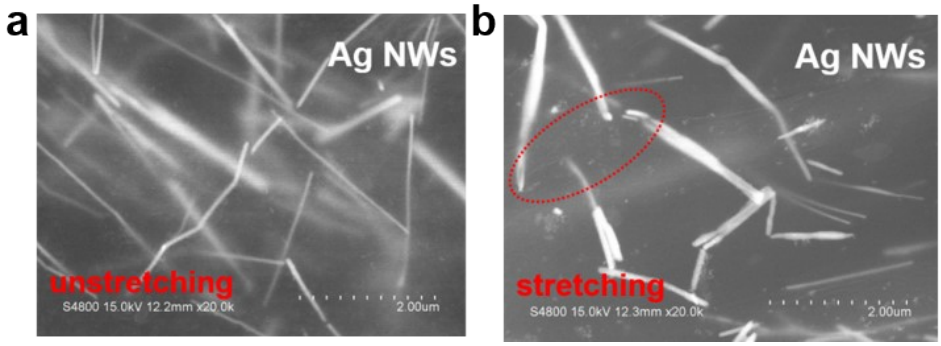

Fig. S15 FESEM images of (a) unstretching and (b) stretching state for ACM/Ag NWs.

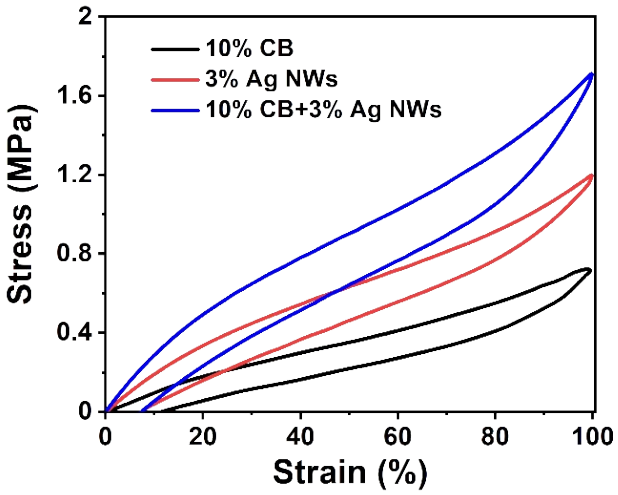

Fig. S16 Stress-strain curves for the ACM films with addition of 10 wt% CB, 3 wt% Ag NWs and 10 wt% CB+3 wt% Ag NWs with the strain limit of 100%. (The speed is 5 mm min^{-1}).

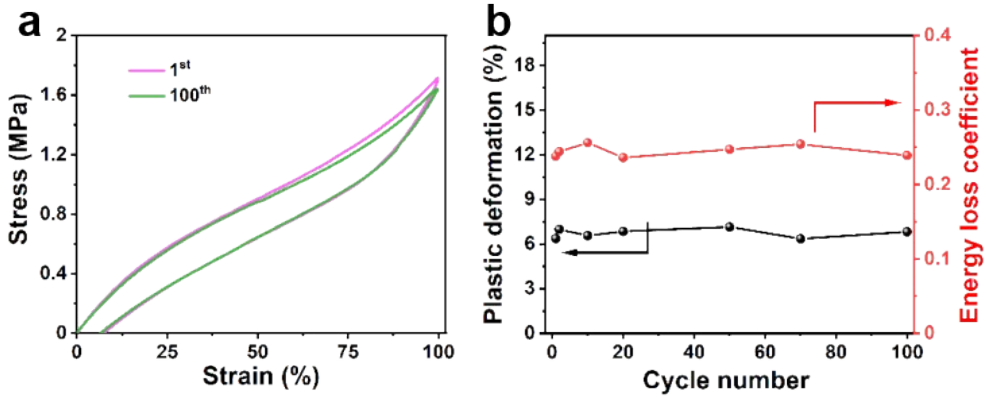

Fig. S17 (a) First and 100th stress-strain curves of ACM/CB-Ag NWs films with the strain limit of 100% (The speed is 5 mm min^{-1}), and (b) Corresponding plastic deformation and energy loss coefficient.

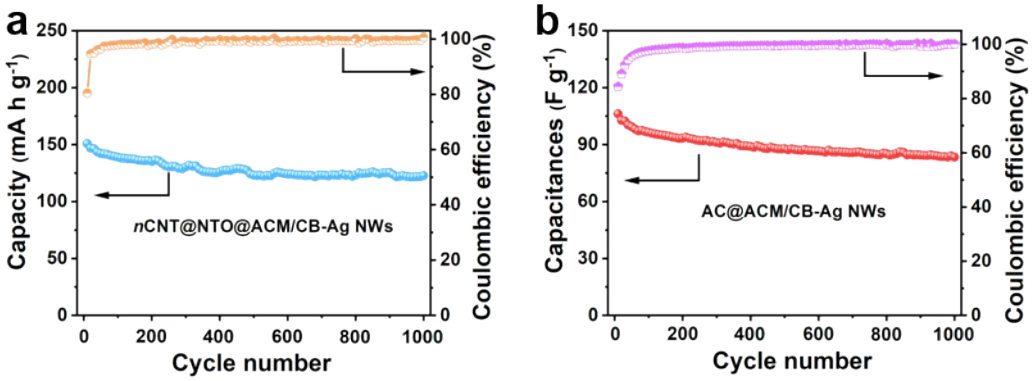

Fig. S18 Long-term cycling performance of (a) *n*CNT@NTO@ ACM/CB-Ag NWs negative electrode at 2 A g^{-1} and (b) AC@ACM/CB-Ag NWs positive electrode at 5 A g^{-1}.

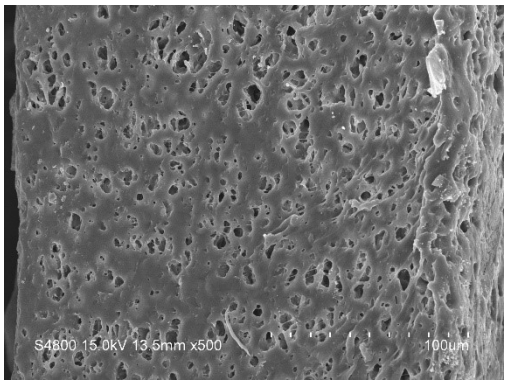

Fig. S19 Cross-sectional FESEM image of BCNF-*p*ACM.

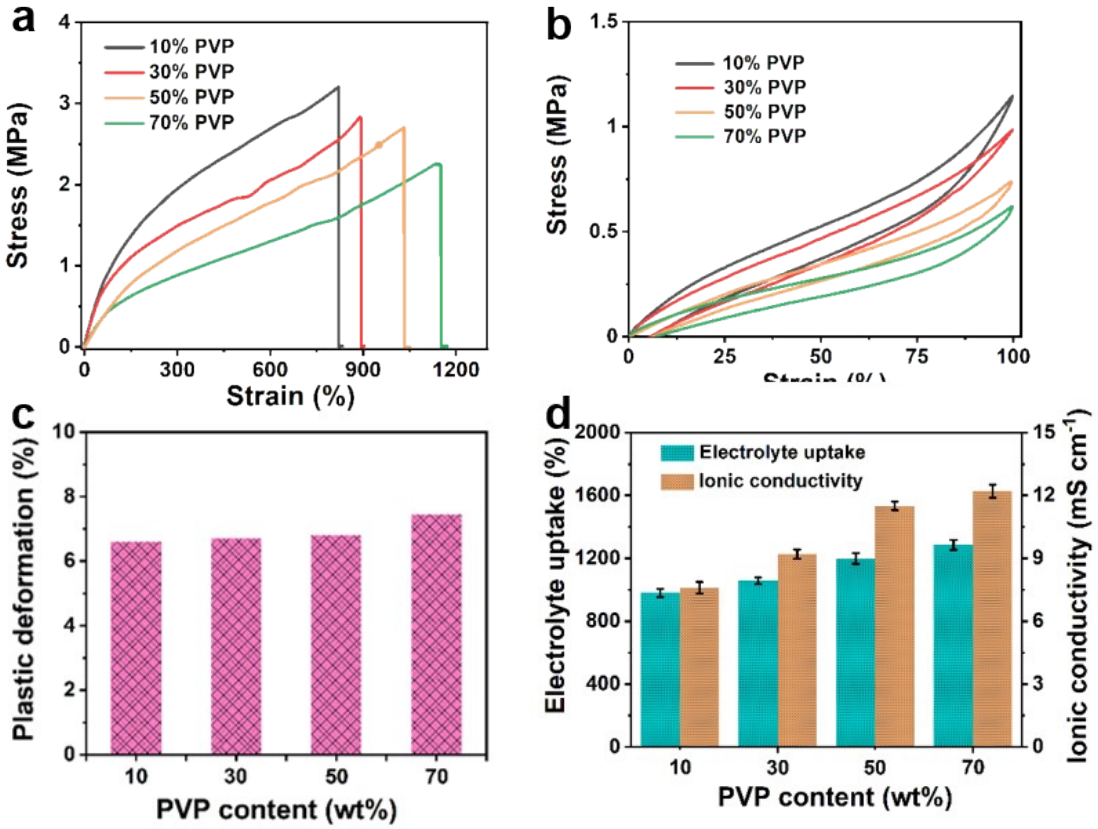

Fig. S20 (a) Stress-strain curves, (b) stress-strain curves and (c) plastic deformation with the strain limit of 100%, and (d) electrolyte uptake and ionic conductivity for the *p*ACM membranes with various PVP content.

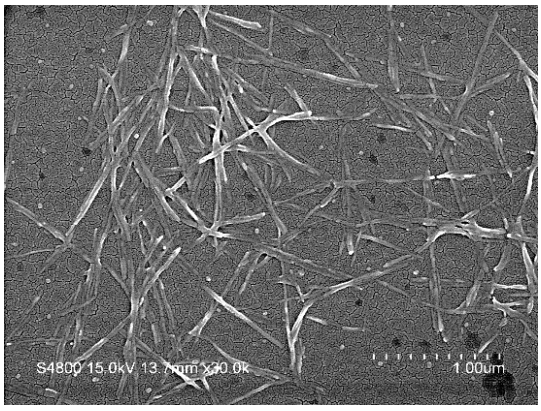

Fig. S21 FESEM image of BCNF prepared by etching of 8M H_2SO_4.

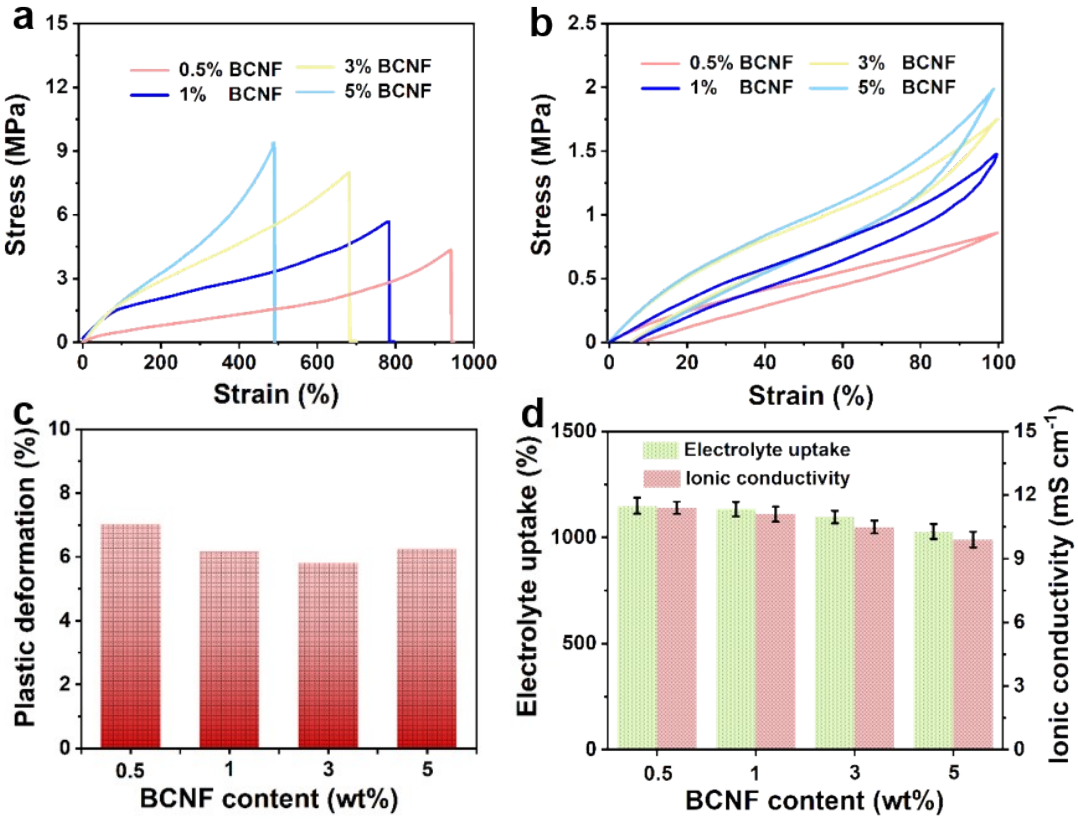

Fig. S22 (a) Stress-strain curves, (b) stress-strain curves and (c) plastic deformation with the strain limit of 100%, and (d) electrolyte uptake and ionic conductivity for the BCNF-*p*ACM membranes with various BCNF content (PVP=50 wt%).

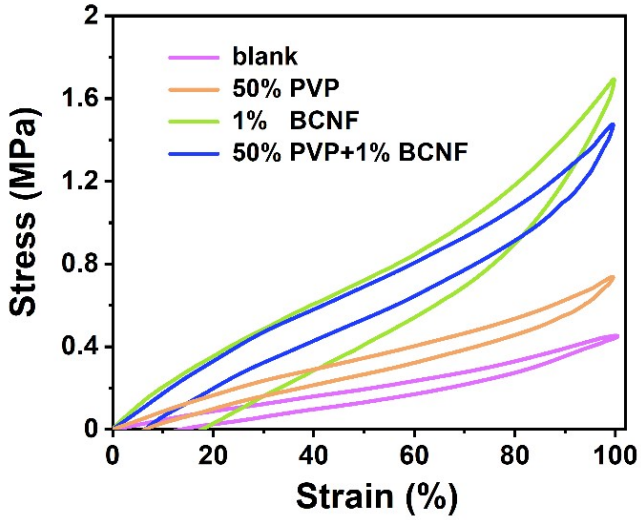

Fig. S23 (a)Stress-strain curves with the strain limit of 100% of ACM (blank), BCNF-ACM (1% BCNF), *p*ACM (50% PVP) and BCNF-*p*ACM (50% PVP+1% BCNF) membranes.

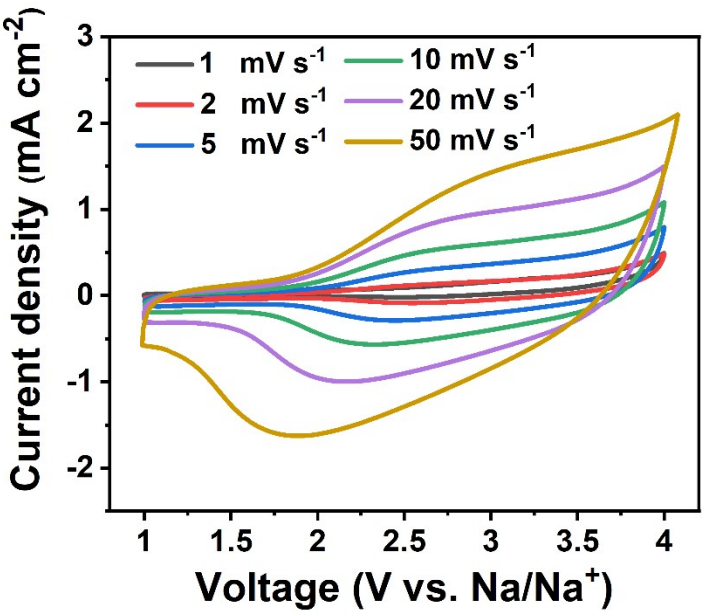

Fig. S24 CV curves of as-assembled SSIC at various scan rates.

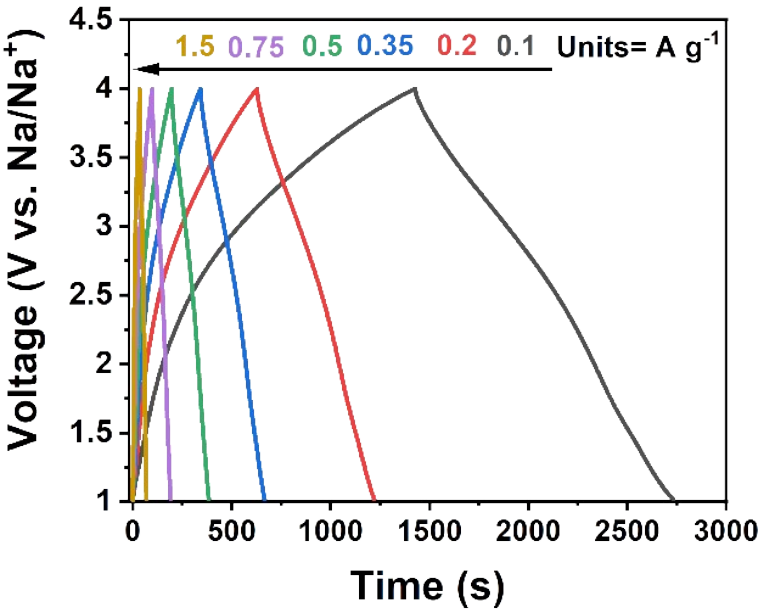

Fig. S25 Galvanostatic charge-discharge curves of SSIC at various current densities.

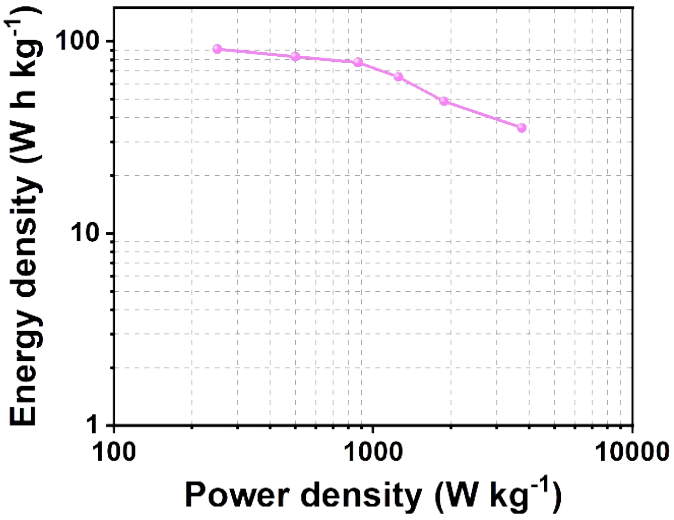

Fig. S26 Ragone plot of as-assembled SSIC based on the mass of total active materials.

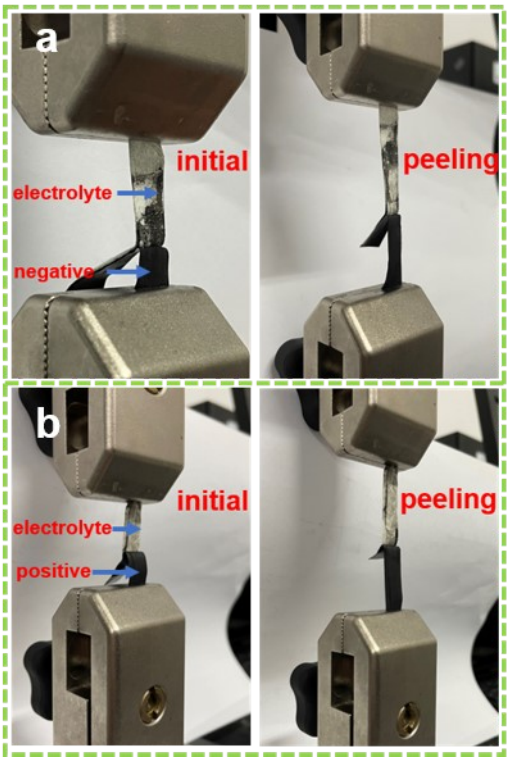

Fig. S27 Digital photos of peel test at initial and peeling state of (a) *n*CNT@NTO@ACM/CB-Ag NWs negative electrode with BCNF-*p*ACM, (b) AC@ACM/CB-Ag NWs positive electrode with BCNF-*p*ACM.